Journal of Bone and Mineral Metabolism (2019) 37:342–350
https://doi.org/10.1007/s00774-018-0926-z

ORIGINAL ARTICLE

Comparison of femur stiffness measured from DXA and QCT for assessment of hip fracture risk

Yunhua Luo[1,2] · **Huijuan Yang**[1]

Received: 20 December 2017 / Accepted: 2 April 2018 / Published online: 18 April 2018

Abstract

Femur stiffness, for example axial and bending stiffness, integrates both geometric and material information of the bone, and thus can be an effective indicator of bone strength and hip fracture risk. Femur stiffness is ideally measured from quantitative computed tomography (QCT), but QCT is not recommended for routine clinical use due to the public concern about exposure to high-dosage radiation. Dual energy X-ray absorptiometry (DXA) is currently the primary imaging modality in clinic. However, DXA is two-dimensional and it is not clear whether DXA-estimated stiffness has adequate accuracy to replace its QCT counterpart for clinical application. This study investigated the accuracy of femur stiffness (axial and bending) estimated from CTXA (computed tomography X-ray absorptiometry) and DXA against those directly measured from QCT. Proximal-femur QCT and DXA from 67 subjects were acquired. For each femur, the QCT dataset was projected into CTXA using CTXA-Hip (Mindways Software, Inc., USA). Femur stiffness at the femoral neck and intertrochanter were then calculated from QCT, CTXA and DXA, respectively, and different elasticity-density relationships were considered in the calculation. Pearson correlations between QCT and CTXA/DXA measured stiffness were studied. The results showed that there were strong correlations between QCT and CTXA derived stiffness, although the correlations were affected by the adopted elasticity-density relationship. Correlations between QCT and DXA derived stiffness were much less strong, mainly caused by the inconsistence of femur orientation in QCT projection and in DXA positioning. Our preliminary clinical study showed that femur stiffness had slightly better performance than femur geometry in discrimination of hip fracture cases from controls.

Keywords Hip fracture risk · Cross-sectional moment of inertia (CSMI) · Femur axial and bending stiffness · Dual energy X-ray absorptiometry (DXA) · Computed tomography X-ray absorptiometry (CTXA)

Introduction

Hip fracture is a common health risk among elderly people worldwide [1–5]. Areal bone mineral density (BMD) measured by dual energy X-ray absorptiometry (DXA) was originally recommended by the World Health Organization (WHO) as a gold standard reference for screening osteoporosis. Later, it was found that there is a strong association between low BMD and fracture outcomes in large populations [6–9]. Therefore, BMD was also adopted as a surrogate of bone strength and used to predict fracture risk. However, the majority of fracture cases have BMD measurements that are in the safe scope specified by WHO [10, 11]. The main reason is that BMD cannot fully represent bone strength, because the latter is determined by the mechanical quality of bone and bone sizes. Although BMD is indeed an indicator of bone strength, information of femur geometry is missing [10]. To consider the effect of bone geometry on fracture risk, hip structure analysis (HSA) tool was developed [12–14] and has been applied in clinical trials [15–17]. By conversion of heterogeneous bone mass distribution into an equivalent homogeneous material, bone geometric parameters such as cross-sectional area (CSA) and cross-sectional moment of inertia (CSMI) consider both bone mass and cross-sectional

✉ Yunhua Luo
Yunhua.Luo@umanitoba.ca

[1] Department of Mechanical Engineering, University of Manitoba, 75A Chancellor's Circle, Winnipeg, MB R3T 2N2, Canada

[2] Department of Biomedical Engineering, University of Manitoba, 75A Chancellor's Circle, Winnipeg, MB R3T 2N2, Canada

geometry. Clinical studies have shown that there indeed exist associations between clinical fracture outcomes and femoral geometry represented by cross-sectional area (CSA) and cross-sectional moment of inertia (CSMI) [15, 16, 18]. However, the contribution of femur geometry to hip fracture prediction over and above BMD is modest [19, 20]. CSA and CSMI were originally introduced in structural mechanics to describe the capability of a beam made of homogeneous material to resist axial and flexural loading [21]. Later, these parameters were extended to reinforced concrete beams, where a rebar is converted into an equivalent amount of concrete using the ratio of rebar and concrete Young's modulus [22, 23]. In hip structure analysis, the above methodology was adopted to consider bone mass inhomogeneity over femur cross-section, an equivalent bone thickness (or the length of X-ray path through bone) is computed from areal BMD measured by DXA and average physical density of bone (1.85 g/cm^3) [13, 14], the latter is the density of bone when it is fully mineralized. The original conversion reference, i.e. Young's modulus, is replaced by bone mass density in hip structure analysis. Nevertheless, extensive in vitro experimental studies have shown that the relationship between bone Young's modulus and bone density is mostly nonlinear [24] with the mathematical form $E = a\rho^b$, where E is Young's modulus, ρ is bone density, a and b are coefficients determined by experiments. Therefore, CSA and CSMI may not be able to represent the actual capability of a femur to resist axial and bending loading.

Femur stiffness considers both geometric and material information and can be a more effective surrogate of femur strength. Previous studies have found strong association between bone stiffness and bone strength [25–27]. Another important aspect of bone strength is fracture toughness [28] which has not been considered in clinical assessment of fracture risk. However, similar to the dilemma in the calculation of femur cross-sectional geometric properties [17, 29–31], femur stiffness is also ideally computed from three-dimensional medical images such as quantitative computed tomography (QCT), but QCT is not recommended for routine examination due to its high radiation dosage and expensive operational cost [32]. Dual energy X-ray absorptiometry (DXA) is currently the most widely available and commonly utilized imaging modality for clinical diagnosis of osteoporosis and will probably remain so in the foreseeable future [33]. Nevertheless, DXA is inherently two-dimensional and does not contain complete information required for the calculation of femur stiffness. To determine whether or not DXA can be used to replace QCT to estimate femur stiffness for clinical application, we first studied the correlations between QCT and DXA derived femur stiffness, and then applied DXA-estimated femur stiffness in the discrimination of clinical hip fracture cases from controls.

Materials and methods

Based on Engineering Mechanics [21, 23], the ability of a beam to resist axial compression/tension and flexural bending are described by its axial and bending stiffness. For a beam made of inhomogeneous material, for example a femur bone, the stiffness must be calculated by integration, i.e.,

$$K_a = \int_A E(x,y)\mathrm{d}A, \qquad K_b^x = \int_A E(x,y)y^2\mathrm{d}A, \qquad K_b^y = \int_A E(x,y)x^2\mathrm{d}A, \tag{1}$$

where $E(x, y)$ is bone local Young's modulus located at point (x, y) on cross-section A. K_b^x and K_b^y are the bending stiffness about two orthogonal axes of the cross-section. For a homogeneous material, Young's modulus is constant, and Eq. (1) degenerates to the commonly used stiffness expressions, i.e. $K_a = EA$, $K_b^x = EI_x$ and $K_b^y = EI_y$, where $A = \int_A \mathrm{d}A$, $I_x = \int_A y^2\mathrm{d}A$, and $I_y = \int_A x^2\mathrm{d}A$ are, respectively, cross-sectional area (CSA) and cross-sectional moments of inertia (CSMI).

To study equivalence between QCT and DXA measured stiffness in the lateral-medial plane, QCT and DXA of left-side proximal-femur from 67 subjects (34 females and 33 males) were acquired. Statistics of the subjects are provided in Table 1.

QCT was scanned using the CT portion of a Biograph 16 PET/CT system (Siemens Medical Solutions, Knoxville, TN, USA). This CT system is equivalent to a Siemens Sensation 16. Images were acquired in spiral mode using a 120 kVp, 175 effective mAs technique with the CARE Dose4D option enabled. The pixel dimensions were 0.48828 (mm) × 0.48828 (mm). DXA was scanned using a clinical Prodigy (GE Healthcare) DXA scanner with the standard scan mode (37.0 μGy).

The femur has a non-circular cross-section and non-uniform mass distribution in the circumferential direction. Therefore, the femur has different bending stiffness in different orientation. Since hip DXA is a projection of the femur in the anteroposterior orientation, hip DXA can only be used to estimate femur bending stiffness in the medial–lateral plane. To compare femur stiffness derived from DXA and QCT, the stiffness from QCT must be computed strictly in the same

Table 1 Statistics of subjects

	Age (years)	Height (cm)	Weight (kg)	Body mass index (kg/m^2)
Mean (std)	64.5 (8.3)	168.7 (9.4)	82.8 (15.6)	29.1 (4.8)
Scope	50–86	124.5–185.5	55.1–126.6	21.0–42.7

orientation that the DXA is projected. This is challenging, because femur standard orientation in DXA scanning is difficult to maintain, and a small internal–external rotation of the femur usually exists [34, 35]. This will affect the calculated stiffness. To eliminate the effect of inconsistent femur orientation, commercial software QCT-Pro and CTXA-Hip (Mindways Software Inc., Austin, USA) was used in our study. CTXA-Hip is able to project femur QCT scans in a specified orientation and produce a two-dimensional image CTXA (computed tomography X-ray absorptiometry) which is equivalent to clinical DXA [36, 37].

Femur stiffness was calculated using pixel-by-pixel integration of Eq. (1). The key step was to compute bone Young's modulus, $E(x, y)$, from pixel values. The method used to compute femur stiffness and to study their correlations is described in Fig. 1.

Calculation of femur stiffness from QCT

To calculate femur stiffness from QCT, femur QCT scans were imported into QCT Pro, femur cross-sections at femoral neck and intertrochanter were reconstructed and exported in the format of DICOM (digital imaging and communications in medicine). A sample of femoral-neck cross-section is shown in Fig. 2a. Pixel-wise volumetric BMD was extracted from the DICOM image using the formula provided by Midways Software Inc.,

$$\rho_{\mathrm{v}}\left(\frac{\mathrm{mg}}{\mathrm{cm}^3}\right) = \frac{c}{k}(CT - b), \tag{2}$$

where $c = 1.073$ is the field uniformity correction (FUC) coefficient, $k = 1.28$ is the CT calibration slope, CT is pixel value in the DICOM image, and $b = -1024$ is the CT calibration intercept.

Bone Young's modulus is obtained by an elasticity-density relationship. A large number of elasticity-density functions have been established by in vitro mechanical testing of bones [24], the majority of the functions are nonlinear. The selection of elasticity-density function definitely has effect on the calculated stiffness and probably also on the correlations. Three mathematically representative elasticity-density relationships were considered in this study. They are labeled, respectively, as material models MM-I, MM-II and MM-III in the following equations:

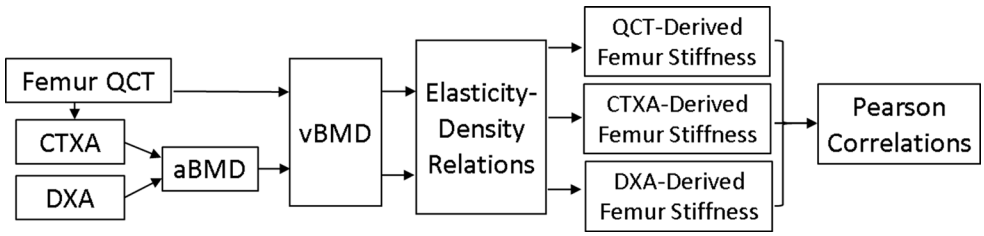

Fig. 1 Study of correlations between QCT and CTXA/DXA derived femur stiffness

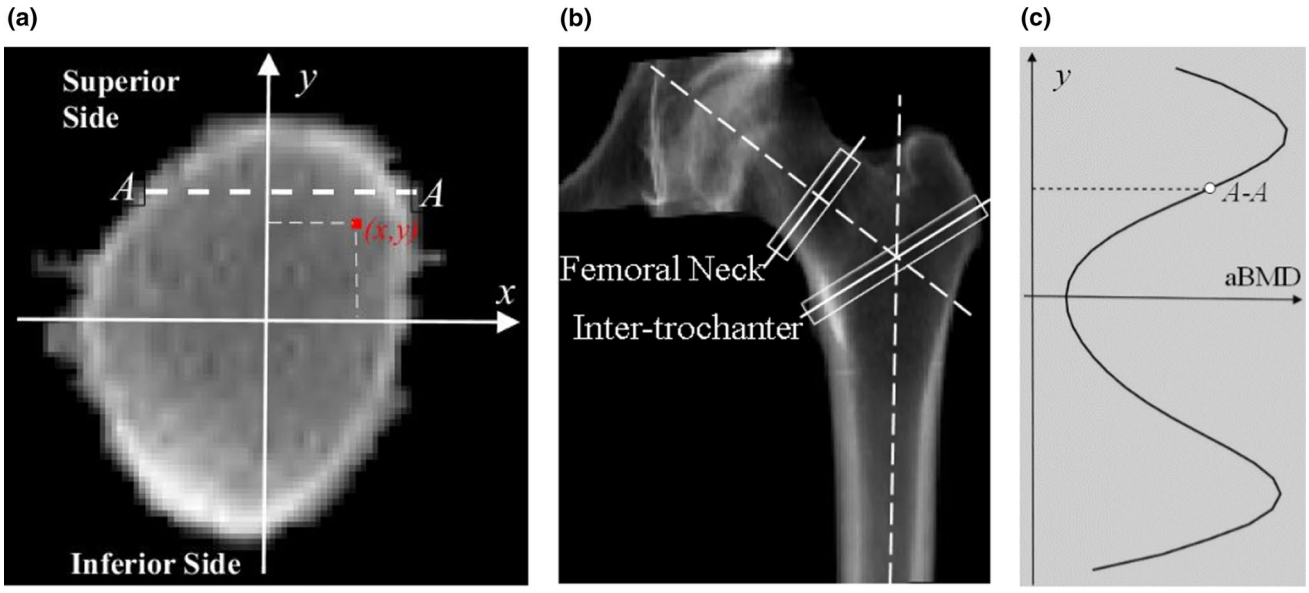

Fig. 2 **a** Cross-section of femoral neck exported from QCT Pro; **b** CTXA projected by CTXA-Hip from QCT scans; **c** areal BMD profile at the femoral neck extracted from CTXA

1. Linear function (MM-I) [38]

$$E(\text{GPa}) = 0.573\rho_{\text{v}} - 0.0094. \quad (3a)$$

2. Exponential function with an exponent between 1 and 2 (MM-II) [39]

$$E(\text{GPa}) = 8.92\rho_{\text{v}}^{1.83}. \quad (3b)$$

3. Exponential function with an exponent larger than 2 (MM-III) [40]

$$E(\text{GPa}) = 2.0173\rho_{\text{v}}^{2.46}. \quad (3c)$$

The bone tissue density (ρ_{v}) in the above functions is apparent density in the unit of gram per cubic centimeter (g/cm^3). It was assumed that bone in compression and in tension has similar Young's modulus [41–43]. Barak et al. [43] demonstrated by electronic speckle pattern interferometry (ESPI) that the tensile Young's modulus of cortical bone is only slightly greater than the compressive Young's modulus.

Estimation of femur stiffness from CTXA and DXA

A sample femur CTXA is displayed in Fig. 2b, the femoral neck cross-section marked in the figure is shown in Fig. 2a (before projection). The projection orientation and cross-section location of QCT scans can be precisely controlled by CTXA-Hip. Therefore, femur stiffness computed from QCT and CTXA are consistent. However, the computation of femur stiffness from CTXA (or DXA) is not as straight forward as from QCT, because CTXA and DXA are projectional (two-dimensional) image and the information required to calculate the stiffness is incomplete. Nevertheless, it is still possible to estimate the stiffness from CTXA or DXA. Consider a composite engineering beam consisting of reinforcement fibers that is intended to resist the moments shown in Fig. 3. Based on engineering beam theory, contributions of the fibers to resisting the moments are determined by their distance from the neutral line, and are independent of their horizontal location. Therefore, the fibers can be replaced by a homogenized material that has an equivalent contribution. A CTXA (or DXA) image can be considered as the result of such a material homogenization in the projectional direction, and theoretically femur stiffness estimated from the resulting CTXA can be equivalent to that derived from the corresponding QCT scans.

Femur stiffness at a cross-section was estimated from CTXA by the following steps. First, areal BMD profile of the cross-section, for example the narrowest femoral neck, was extracted from CTXA. One sample profile is shown in Fig. 2c. Areal BMD along a projection line (e.g. line A–A in Fig. 2) was converted to volumetric BMD using the following equation [44]

$$\rho_{\text{V}} = 1.20 \times \frac{\rho_{\text{A}}}{W_{\text{neck}}} + 0.0242. \quad (4)$$

In the above equation, ρ_{A} is areal or projected BMD, W_{neck} is the width at the narrowest femoral neck. The equation was established by linear regression of volumetric BMD measured by QCT Pro and areal BMD measured by CTXA-Hip.

Femur thickness along the projection line A–A was estimated by [13, 14]

$$t = \frac{\rho_{\text{A}}}{1.85}. \quad (5)$$

Young's modulus was calculated using Eqs. (3a–3c) and (4). Femur stiffness at a cross-section was integrated from the areal BMD profile based on Eq. (1), and the integration area (dA) was taken as the product of pixel height and the thickness estimated by Eq. (5).

Clinical cohort for discrimination test

The ability of femur stiffness and geometric properties to discriminate hip fracture cases from controls were tested and compared by a clinical cohort. The cohort consisted of 393 women, including 99 prior hip fractures and 294 controls. In the cohort selection, the following criteria were applied: (1) women age ≥ 65 years; (2) femoral neck T-score below − 1; and (3) no osteoporosis treatment. The clinical data of the subjects are provided in Table 2.

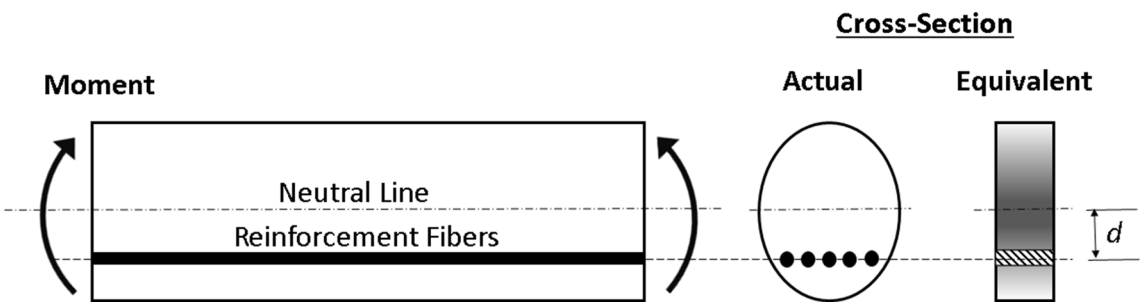

Fig. 3 Equivalent cross-section produced by material projection

Table 2 Statistics of fracture and control group

	Fracture group	Control group
Age (years)	78 ± 9	74 ± 12
Femoral neck *T*-score	−2.4	−2.3

For each subject in the cohort, DXA of left hip was acquired. Femur stiffness was calculated using the previously described equations. Femur cross-sectional geometric properties, including cross-sectional area (CSA) and cross-sectional moment of inertia (CSMI), were calculated from CTXA or DXA images using the formulas proposed by Martin et al. [45], Beck et al. [13] and Yoshikawa et al. [14].

$$\mathrm{CSA} = h\sum_{i=1}^{N} t_i \quad (\text{in cm}^2), \tag{6a}$$

$$\mathrm{CSMI} = h\sum_{i=1}^{N} y^2 t_i \quad (\text{in cm}^4). \tag{6b}$$

In the above equations, h is the pixel height that is determined by the imaging resolution; t_i is the femur thickness along the path A–A in Fig. 2a and it was estimated by Eq. (5); y is the distance between the considered pixel and the neutral axis; N is the number of pixels along a femur cross-section in CTXA or DXA image.

The discrimination performance was assessed using the area under the receiver operating characteristic curve (AUC) and age-adjusted odds ratio (OR per SD decrease) in logistic regression models.

Results

Pearson correlations between QCT and CTXA/DXA derived femur stiffness/geometric properties are presented in Table 3. The properties were calculated at the femoral-neck and inter-trochanteric cross-section as shown in Fig. 2b. The following observations can be made from the results:

1. All the correlations presented in Table 3 are statistically significant ($p < 0.001$).
2. Correlations between QCT and CTXA derived properties (both stiffness and geometry) are much stronger than those between QCT and DXA.
3. The strength of correlations between QCT and CTXA/DXA derived stiffness is affected by material models, with the strongest correlations produced by MM-I and the weakest by MM-III. For material model MM-I, the stiffness and geometric properties have the same correlation strengths.

Correlations and Bland–Altman plots of CTXA and QCT derived flexural and axial stiffness at femoral neck are displayed in Fig. 4. The results were calculated using material model MM-II.

Results of the discrimination test are provided in Table 4. The results show that,

1. With material model MM-I, femur-neck stiffness and geometric property basically had the same performance.
2. The other two material models, MM-II and MM-III, more or less improved the performance of femur stiffness. Femur-neck stiffness with MM-II had the best performance in the discrimination tests.

Table 3 Pearson correlations between QCT and CTXA/DXA and derived femur stiffness/geometry/BMD properties

Cross-section	Image	Stiffness with different material model				Geometry*		CTXA-DXA areal BMD*
			MM-I*	MM-II*	MM-III*			
Femoral neck	CTXA	Bending	0.95	0.93	0.91	CSMI	0.95	0.95
	DXA		0.75	0.73	0.70		0.75	
	CTXA	Axial	0.79	0.71	0.64	CSA	0.79	
	DXA		0.68	0.62	0.57		0.68	
Inter-trochanter	CTXA	Bending	0.88	0.87	0.86	CSMI	0.88	0.94
	DXA		0.73	0.70	0.67		0.73	
	CTXA	Axial	0.83	0.81	0.77	CSA	0.83	
	DXA		0.70	0.68	0.61		0.70	

*$p < 0.001$

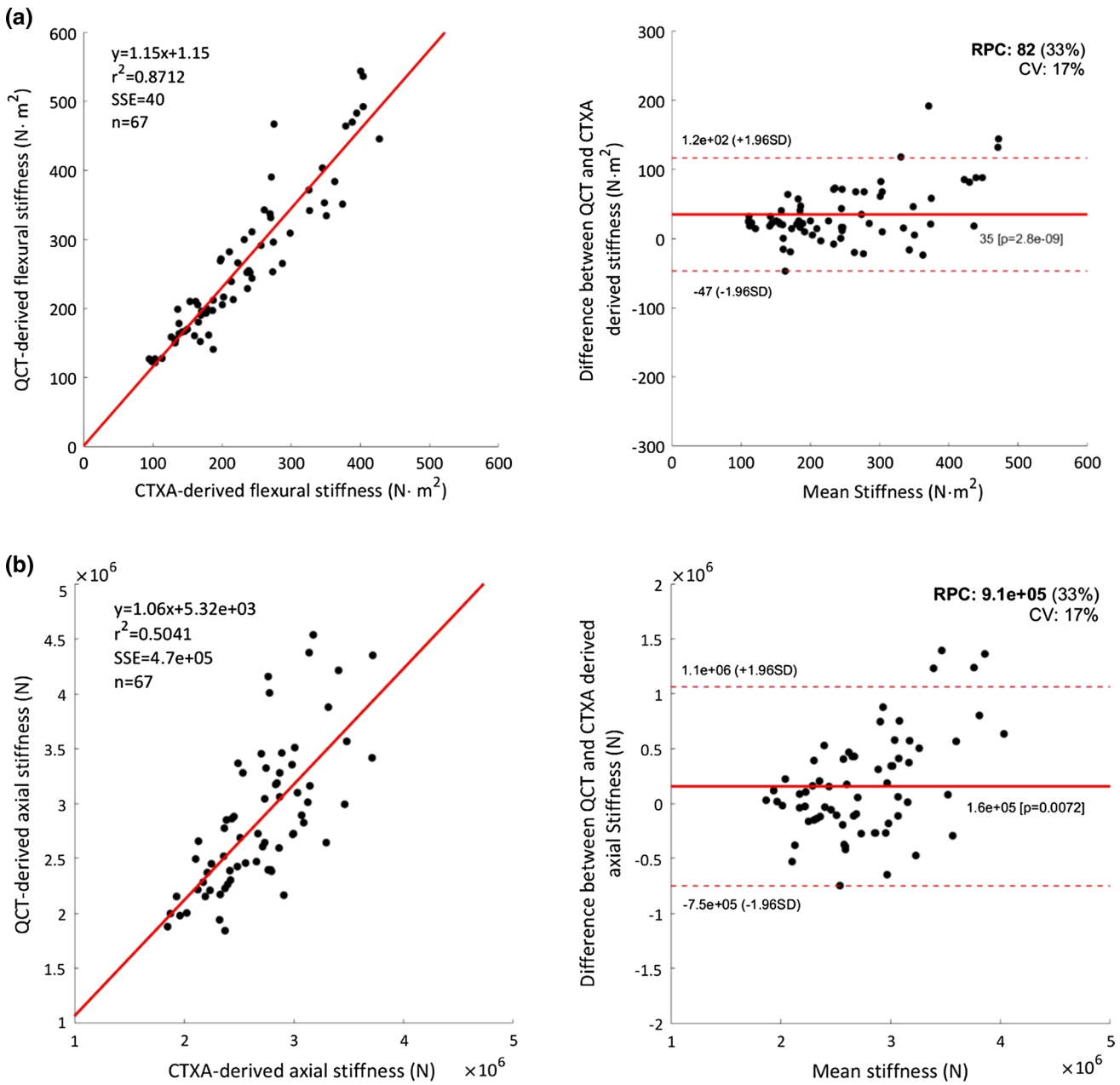

Fig. 4 plot of CTXA and QCT derived stiffness with material model MM-II

Discussion

Correlations between areal BMD values measured from CTXA and DXA (shown in the last column of Table 3) were very strong and similar to those reported by Cann et al. [37] and Khoo et al. [36]. The strong correlation is mainly attributed to the fact that, the areal BMD is taken as an average over a region of interest (ROI), and is thus less sensitive to inconsistence of femur orientation caused by femur internal–external rotation [34, 35]. Theoretically, femur mechanical properties derived from CTXA and DXA should be equivalent.

The large differences between QCT-CTXA and QCT-DXA correlations in Table 3 were mainly caused by inconsistence orientation used in QCT and DXA computation of the cross-sectional properties. A femur cross-section is non-circular and has different mechanical properties in different orientation, for example, the femoral-neck cross-section shown in Fig. 2a has different bending stiffness about x and y axis. A slight internal–external rotation of the femur in DXA scanning will project the concerned cross-section in different

Table 4 AUC and age-adjusted OR of femur geometry/stiffness in discrimination test

Femur-neck geometry/stiffness	AUC (95% CI)	Age-adjusted OR (95% CI)
Cross-section area (CSA)	0.723 (0.662, 0.784)	2.34 (1.75, 3.15)
Axial stiffness (K_a)		
MM-I	0.723 (0.662, 0.783)	2.35 (1.76, 3.16)
MM-II	0.734 (0.672, 0.795)	2.42 (1.80, 3.26)
MM-III	0.729 (0.668, 0.789)	2.38 (1.79, 3.19)
Cross-section moment of inertia (CSMI)	0.602 (0.529, 0.674)	1.42 (1.08, 1.85)
Bending stiffness (K_b^x)		
MM-I	0.602 (0.529, 0.674)	1.42 (1.08, 1.85)
MM-II	0.632 (0.560, 0.704)	1.63 (1.24, 2.15)
MM-III	0.617 (0.544, 0.689)	1.50 (1.16, 1.94)
Femoral neck BMD	0.71 (0.650, 0.771)	2.16 (1.81, 2.57)

orientation, and the actual orientation is difficult to determine. The subject has to be re-positioned in DXA and QCT scanning. For the above reason, femur cross-sectional properties calculated from QCT and DXA are more or less from different orientation. Orientation consistence between QCT and CTXA is controlled and ensured by the software. This explains why QCT-CTXA correlations are much stronger than QCT-DXA correlations (Table 3). Reported studies also show that correlations between QCT and DXA derived geometric properties (CSMI and CSA) are significantly affected by the consistence of femur orientation. In the study conducted by Ramamurthi et al. [17], four DXA images acquired at different angles were co-registered with the QCT dataset to find out the most consistent orientation for the calculation of femur geometric properties, and strong correlations ($r = 0.93$–0.95, $p < 0.001$) were achieved. In other similar studies [30, 31, 46], femur orientation consistence was not strictly controlled, and the correlations were, therefore, much weaker and had large variations ($r = 0.7$–0.9).

In addition to the effect of femur orientation, correlations between QCT and CTXA/DXA derived femur stiffness were also affected by bone elasticity-density relationship (Table 3). It is not surprising that for a linear relationship such as MM-I in Eq. (3a), the stiffness computed from QCT and CTXA/DXA had the same correlation strength as the geometric properties, because the relationships used in the derivation of both stiffness and geometric properties are linear. However, with the adoption of nonlinear relationships such as MM-II and MM-III, the strength of stiffness correlations decreased, although they were still strong and statistically significant. There exist positive correlations between the difference and mean of axial and bending stiffness, as can be observed from the Bland–Altman plots in Fig. 4. This phenomenon was caused by the nonlinear elasticity-density relationship. Theoretically, for the exponential function in Eq. (3b), the same difference in vBMD (between CTXA estimated and QCT measured) will be amplified more with a higher vBMD than with a lower vBMD. While a higher vBMD will produce larger Young's modulus, and consequently larger axial and bending stiffness.

As shown by the results in Table 4, femur stiffness generally had equal or better performance than femur geometric properties (CSA and CSMI) in the discrimination test. The reason is that femur stiffness considers both bone material and geometric properties and it is a better surrogate of bone strength than the geometric properties. Femur stiffness computed from material model MM-II had better performance than from the other two types of relationships, which may imply that MM-II or the similar elasticity-density relationships more realistically describes bone elasticity. Relationships between bone mechanical properties and bone density are very complicated and have not been fully understood. Although a large number of elasticity-density relationships have been established by in vitro bone mechanical testing [24, 47], it is difficult to determine which one is more accurate than the others, because the relationships were developed using different experimental methods and bone specimens taken from different subjects at different anatomic sites. Nevertheless, the majority of the established relationships are in the form of exponential function with an index between 1 and 2. However, the discrimination ability of femur stiffness is still limited. Based on Table 4, bending stiffness (K_b^x) had greater AUC than CSMI ($p = 0.03$), but both had smaller AUC than femoral neck BMD; The AUC for axial stiffness (K_a) was slightly greater than for CSA, but the difference was not significant ($p > 0.2$). The primary reason is that hip fracture is jointly determined by femur strength and impact force induced in fall [48], femur stiffness is only a surrogate of bone strength instead of the real strength and fall-induced impact force has not been considered yet. Second, femur stiffness estimated from DXA is not accurate for a number of reasons. Cortical and trabecular bone have different mechanical properties but they cannot be separated in a DXA image. Bone density required by the material models in Eq. (3a–3c) is pointwise density, but the density estimated by Eq. (4) is an average of bone

mass along the projection path. Femur thickness estimated by Eq. (5) is not accurate either. All of the above factors affected the accuracy of femur stiffness estimated from DXA.

In conclusion, femur stiffness estimated from DXA is equivalent to those measured from QCT. DXA-derived femur stiffness (axial and bending) has stronger association with hip fracture than femur geometry (CSA and CSMI).

Acknowledgements The reported research has been supported by the Natural Sciences and Engineering Research Council (NSERC) and the Manitoba Health Research Council (MHRC) in Canada, which are gratefully acknowledged. Thanks to Winnipeg Health Science Centre for providing the QCT and DXA images used in this study.

Funding Funding was provided by Natural Sciences and Engineering Research Council of Canada (Grant no: 37098) and Research Manitoba (Grant no: 37807).

Compliance with ethical standards

Ethical approval The use of medical images in this study was approved by the Research Ethics Committee at the University of Manitoba, Canada.

Conflict of interest None of the authors had any personal or financial conflicts of interest.

References

1. Boonen S, Autier P, Barette M, Vanderschueren D, Lips P, Haentjens P (2004) Functional outcome and quality of life following hip fracture in elderly women: a prospective controlled study. Osteoporos Int 15:87–94
2. Brunner LC, Eshilian-Oates L, Kuo TY (2003) Hip fractures in adults. Am Fam Physician 67:537–543
3. Abrahamsen B, van Staa T, Ariely R, Olson M, Cooper C (2009) Excess mortality following hip fracture: a systematic epidemiological review. Osteoporos Int 20:1633–1650
4. Alvarez-Nebreda ML, Jimenez AB, Rodriguez P, Serra JA (2008) Epidemiology of hip fracture in the elderly in Spain. Bone 42:278–285
5. Brauer CA, Coca-Perraillon M, Cutler DM, Rosen AB (2009) Incidence and Mortality of Hip Fractures in the United States. J Am Med Assoc 302:1573–1579
6. Marshall D, Johnell O, Wedel H (1996) Meta-analysis of how well measures of bone mineral density predict occurrence of osteoporotic fractures. BMJ 312:1254–1259
7. Barrett-Connor E, Siris ES, Wehren LE, Miller PD, Abbott TA, Berger ML, Santora AC, Sherwood LM (2005) Osteoporosis and fracture risk in women of different ethnic groups. J Bone Miner Res 20:185–194
8. Cranney A, Jamal SA, Tsang JF, Josse GR, Leslie WD (2007) Low bone mineral density and fracture burden in postmenopausal women. CMAJ 177:575–580
9. McClung MR (2005) The relationship between bone mineral density and fracture risk. Curr Osteoporos Rep 3:57–63
10. Cefalu CA (2004) Is bone mineral density predictive of fracture risk reduction? Curr Med Res Opin 20:341–349
11. Unnanuntana A, Gladnick BP, Donnelly E, Lane JM (2010) The assessment of fracture risk. J Bone Jt Surg Am 92:743–753
12. Beck TJ (2007) Extending DXA beyond bone mineral density: understanding hip structure analysis. Curr Osteoporos Rep 5:49–55
13. Beck TJ, Ruff CB, Warden KE, Scott WW Jr, Rao GU (1990) Predicting femoral neck strength from bone mineral data: a structural approach. Invest Radiol 25:6–18
14. Yoshikawa T, Turner CH, Peacock M, Slemenda CW, Weaver CM, Teegarden D, Markwardt P, Burr DB (1994) Geometric structure of the femoral neck measured using dual-energy X-ray absorptiometry. J Bone Miner Res 9:1053–1064
15. Mochizuki T, Yano K, Ikari K, Kawakami K, Hiroshima R, Koenuma N, Ishibashi M, Shirahata T (2016) Hip structure analysis by DXA of teriparatide treatment: a 24-month follow-up clinical study. J Orthop 13:414–418
16. Beck TJ, Looker AC, Ruff CB, Sievanen H, Wahner HW (2000) Structural trends in the aging femoral neck and proximal shaft: analysis of the Third National Health and Nutrition Examination Survey dual-energy X-ray absorptiometry data. J Bone Miner Res 15:2297–2304
17. Ramamurthi K, Ahmad O, Engelke K, Taylor RH, Zhu K, Gustafsson S, Prince RL, Wilson KE (2012) An in vivo comparison of hip structure analysis (HSA) with measurements obtained by QCT. Osteoporos Int 23:543–551
18. Mayhew P, Kaptoge S, Loveridge N, Power J, Kroger HP, Parker M, Reeve J (2004) Discrimination between cases of hip fracture and controls is improved by hip structural analysis compared to areal bone mineral density. An ex vivo study of the femoral neck. Bone 34:352–361
19. Ahlborg HG, Nguyen ND, Nguyen TV, Center JR, Eisman JA (2005) Contribution of hip strength indices to hip fracture risk in elderly men and women. J Bone Miner Res 20:1820–1827
20. Kaptoge S, Beck TJ, Reeve J Stone KL, Hillier TA, Cauley JA, Cummings SR (2008) Prediction of incident hip fracture risk by femur geometry variables measured by hip structural analysis in the study of osteoporotic fractures. J Bone Miner Res 23:1892–1904
21. Timoshenko S, Goodier JN (1951) Theory of elasticity. McGraw-Hill Book Company Inc, New York
22. Wight JK, MacGregor JG (2012) REINFORCED CONCRETE—mechanics and design. Pearson, London
23. Hartsuijker C, Welleman JW (2007) Engineering mechanics. Springer, New York
24. Helgason B, Perilli E, Schileo E, Taddei F, Brynjólfsson S, Viceconti M (2008) Mathematical relationships between bone density and mechanical properties: a literature review. Clin Biomech 23:135–146
25. Borders S, Petersen KR, Orne D (1977) Prediction of bending strength of long bones from measurements of bending stiffness and bone mineral content. J Biomed Eng 99:40–44
26. Keaveny TM, Wachtel EF, Ford CM, Hayes WC (1994) Differences between the tensile and compressive strengths of bovine tibial trabecular bone depend on modulus. J Biomech 27:1137–1146
27. Yeni YN, Dong XN, Fyhrie DP, Les CM (2004) The dependence between the strength and stiffness of cancellous and cortical bone tissue for tension and compression: extension of a unifying principle. Biomed Mater Eng 14:303–310
28. Ritchie RO, Koester KJ, Ionova S, Yao W, Lane NE, Ager JW III (2008) Measurement of the toughness of bone: a tutorial with special reference to small animal studies. Bone 43:798–812
29. Ahmad O, Ramamurthi K, Bouxsein ML, Engelke K, Wilson KE, Taylor RH (2009) Evaluation of 3D structural properties of the proximal femur using multiple 2D DXA images and a statistical atlas. J Clin Densitom 12:111–112

30. Ohnaru K, Sone T, Tanaka K, Akagi K, Ju Y-I, Choi H-J, Tomomitsu T, Fukunaga M (2013) Hip structural analysis: a comparison of DXA with CT in postmenopausal Japanese women. Springerplus 2:331
31. Prevrhal S, Shepherd JA, Faulkner KG, Gaither KW, Black DM, Lang TF (2008) Comparison of DXA hip structural analysis with volumetric QCT. J Clin Densitom 12:232–236
32. Engelke K, Lang T, Khosla S, Qin L, Zysset P, Leslie WD, Shepherd JA, Schousboe JT (2015) Clinical use of quantitative computed tomography (QCT) of the hip in the management of osteoporosis in adults: the 2015 ISCD official positions—part I. J Clin Densitom 18:338–358
33. Adams JE (2013) Advances in bone imaging for osteoporosis. Nat Rev Endocrinol 9:28–42
34. Lekamwasam S, Lenora RSJ (2003) Effect of leg rotation on hip bone mineral density measurements. J Clin Densitom 6:331–336
35. Goh JC, Low SL, Bose K (1995) Effect of femoral rotation on bone mineral density measurements with dual energy X-ray absorptiometry. Calcif Tissue Int 57:340–343
36. Khoo BC, Brown K, Cann C, Zhu K, Henzell S, Low V, Gustafsson S, Price RI, Prince RL (2009) Comparison of QCT-derived and DXA-derived areal bone mineral density and t scores. Osteoporos Int 20:1539–1545
37. Cann CE, Adams JE, Brown JK, Brett AD (2014) CTXA hip—an extension of classical DXA measurements using quantitative CT. PLoS ONE 9(3):e91904
38. Li B, Aspden RM (1997) Composition and mechanical properties of cancellous bone from the femoral head of patients with osteoporosis or osteoarthritis. J Bone Miner Res 12:641–651
39. Morgan EF, Bayraktar HH, Keaveny TM (2003) Trabecular bone modulus–density relationships depend on anatomic site. J Biomech 36:897–904
40. Dalstra M, Huiskes R, Odgaard A, van Erning L (1993) Mechanical and textural properties of pelvic trabecular bone. J Biomech 26:523–535
41. Currey JD (1969) The relationship between the stiffness and the mineral content of bone. J Biomech 2:477–480
42. Currey JD (1969) The mechanical consequences of variation in the mineral content of bone. J Biomech 2:1–11
43. Barak MM, Currey JD, Weiner S, Shahar R (2009) Are tensile and compressive young's moduli of compact bone different? J Mech Behav Biomed Mater 2:51–60
44. Luo Y (2018) Empirical functions for conversion of femur areal and volumetric bone mineral density. J Biomed Biol Eng. https://doi.org/10.1007/s40846-018-0394-x
45. Martin RB, Burr DB (1984) Non-invasive measurement of long bone cross-sectional moment of inertia by photon absorptiometry. J Biomech 17:195–201
46. Danielson ME, Beck TJ, Karlamangla AS, Greendale GA, Atkinson EJ, Lian Y, Khaled AS, Keaveny TM, Kopperdahl D, Ruppert K, Greenspan S, Vuga M, Cauley JA (2013) A comparison of DXA and CT based methods for estimating the strength of the femoral neck in post-menopausal women. Osteoporos Int 24:1379–1388
47. Knowles NK, Reeves JM, Ferreira LM (2016) Quantitative computed tomography (QCT) derived bone mineral density (BMD) in finite element studies: a review of the literature. J Exp Orthop 3:1–16
48. Luo Y (2017) Image-based multilevel biomechanical modeling for fall-induced hip fracture. Springer, New York